Large-Scale Simulations of Novel Materials and Processes

M. Buongiorno Nardelli, J. Bernholc, E. L. Briggs, J.-L. Fattebert,
D. Orlikowski, C. Roland, W. G. Schmidt and Q. Zhao
NC State University, Raleigh, NC 27695-8202

Abstract

Recent advances in theoretical methods combined with the advent of massively-parallel supercomputers allow one to reliably simulate the properties of complex materials from first principles. During the past year we have focused on two important applications: (i) mechanical properties and quantum transport in nanotubes, and (ii) surface optical response of semiconductors for real-time growth diagnostics and feedback control.

Carbon nanotubes are one of the most interesting new materials to emerge in the past decade, with outstanding mechanical and electrical properties. Through a combination of ab initio, tight binding and classical simulations, we have investigated the interplay between mechanical deformations and electronic response, in the aim of characterizing ther behavior in an actual nanomechanical device.

Turning to semiconductor surfaces, we have focused primarily on theoretical calculations of the reflectance difference spectra (RDS) of reconstructed III-V semiconductor surfaces. We have used a massively parallel real-space multigrid technique and an approximate GW treatment to compute the optical signatures of major surface structures of hydrogenated silicon surfaces. These optical fingerprints can be used for feedback control of growth processes with nearly monolayer resolution.

Mechanical deformations and electronic response in carbon nanotubes.

The field of carbon nanotubes has seen an explosive growth in the recent years due to the substantial promise of these molecular structures for the use as high-strength, light-weight materials, superstrong fibers, novel nanometer scale electronic and mechanical devices, catalysts, and as energy storage media.

Carbon nanotubes have already demonstrated exceptional mechanical properties: the excellent resistance to damage during bending has already been widely observed experimentally and studied theoretically.

In the past, we have focused on the theoretical analysis of the mechanism of strain release in carbon nanotubes under uniaxial tension, in an effort to address the question of the ultimate strength of these nanostructures. We have analyzed the transformations leading to

mechanical failure under a tensile load and identified the first stages of the mechanical yield of carbon nanotubes. Novel, unforeseen patterns in plasticity and breakage were observed. Our study, based on the extensive use of ab-initio molecular dynamics simulations, shows that beyond a critical value of the tension, at about 5% strain, an armchair nanotube releases its excess strain via a spontaneous rotation of a C-C bond, which leads to a so-called (5-7-7-5) defect, which consists of two pentagons and two heptagons coupled in pairs [1]. The resulting appearance of a (5-7-7-5) defect can be interpreted as a nucleation of a degenerate dislocation loop in the hexagonal graphitic network. The configuration of this primary dipole is a (5-7) core attached to an inverted (7-5) core.
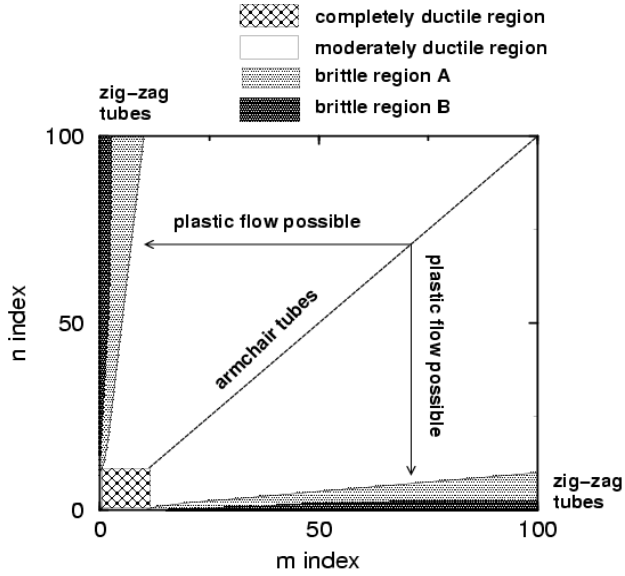

Figure 1: Ductile-brittle domain map for carbon nanotubes with diameters up to 13 nm. Different shaded areas correspond to different possible behaviors (see text).

From our calculations we have been able to identify the full range of elastic responses in strained carbon nanotubes. In particular, under high strain and low temperature conditions, all tubes are brittle. If, on the contrary, external conditions favor plastic flow, such as a low strain and a high temperature, (n,m) tubes with n,m < 14 can be completely ductile, while larger tubes are moderately or completely brittle depending on their symmetry. These results are summarized in Fig. 1, where a map of the ductile *vs.* brittle behavior of a general (n,m) carbon nanotube under an axial tensile load is presented. There are four regions indicated by the different shadings. The small hatched area near the origin is the region of complete ductile behavior, where the formation of (5-7-7-5) defects is always favored under sufficiently large strain. In particular, plastic flow will transform the tube section between the dislocation cores along definite pat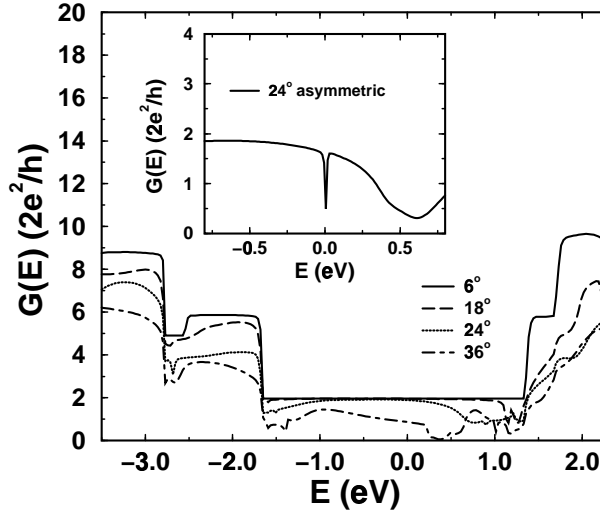hs along the tube walls. During the transformations, the symmetry will change between the armchair and the zigzag type. The same transformations will occur in the larger (white) moderately ductile region. Tubes with indices in this area are ductile, but the plastic behavior is limited by the brittle regions near the axes. Tubes that belong to the last two regions will always follow a brittle fracture path with formation of disordered cracks and large open rings under high tensile strain conditions.

Understanding the response of carbon nanotubes to large deformations is of vital importance for device design. Usually, the positioning of an individual nanotube on the circuit base can be attained via manipulation with a scanning probe tip [2], or by utilizing strong adhesive forces between the NT and the substrate. These procedures are likely to introduce large mechanical deformations in the nanotube, which will modify the geometry and the electronic and transport behavior of the system.

Recently, there has been a great amount of interest in quantum conductance properties of carbon nanotubes. Their electronic and conducting properties have been studied both

Figure 2: Conductance of a symmetrically bent (5,5) armchair nanotube. Different curves correspond to different bending angles: $6°, 18°, 24°$ and $36°$, as shown in the legend. Inset: conductance of a (5,5) tube with an asymmetric bend of $24°$. A pseudo-gap at the Fermi energy (always taken as reference) is clearly present, see text.

experimentally and theoretically [3, 4, 5, 6, 7, 8, 9, 10, 11, 12, 13]. In particular, the sensitivity of the electronic properties of nanotubes to their geometrical structure makes them truly unique in offering the possibility of studying quantum transport in a very tunable environment. To address the issue of quantum transport in carbon nanotubes, we have used a recently developed Green's function-based technique that is very efficient when used with any general Hamiltonian that can be effectively represented within a basis of localized orbitals [14].

We begin with the analysis of the electrical behavior of bent nanotubes. It has recently been observed [4] that in individual carbon nanotubes deposited on a series of electrodes three classes of behavior can be distinguished: (i) non-conducting at room temperature and below, (ii) conducting at all temperatures, and (iii) partially conducting. The last class represents NT's that are conducting at a high temperature but at a low temperature behave as a chain of quantum wires connected in series. It has been argued that the local barriers in the wire arise from bending of the tube near the edge of the electrodes.

Single-walled carbon nanotubes are either metallic or semiconducting depending on their helicity, which is denoted by a pair of integers (n, m). In particular, they are predicted to be metallic if $n - m = 3q$ with $q =$ integer [15]. While armchair NT's are always metallic, diameter plays an important role in modifying the electronic properties of chiral and zigzag NT's. In particular, in small diameter NT's, the hybridization of s and p orbitals of carbon can give rise to splitting of the π and π^* bands responsible for metallicity [16]. For example, $(3q, 0)$ zigzag nanotubes of diameters up to 1.5 nm are always small gap semiconductors, even in the absence of deformations, and can be assigned to the (i) class of behavior of Ref. [4], together with the naturally insulating NT's $(n - m \neq 3q)$.

In Fig. 2 we show the conductance of a (5,5) armchair nanotube ($d = 0.7$ nm) that has been symmetrically bent at angles $\theta = 6°, 18°, 24°, 36°$. θ measures the inclination of the two

ends of the tubes with respect to the unbent axis. No topological defects are present in the tubes. For θ larger than 18° the formation of a kink is observed, which is a typical signature of large-angle bending in carbon nanotubes. Although armchair tubes are always metallic because of their particular band structure, the kink is expected to break the degeneracy of the π and π^* orbitals, thus opening a pseudo-gap in the conductance spectrum [17]. However, if the bending is symmetric with respect to the center of the tube, the presence of the kink does not drastically alter the conductance of the system [13], since the accidental mirror symmetry imposed on the system allows the bands to cross. When this accidental symmetry is lifted, a small pseudo-gap ($\approx$ 6 meV) occurs for large bending angles ($\theta \geq 24°$), see the inset of Fig. 2. The same calculations have been repeated for a (10,10) tube ($d = 1.4$ nm), and no pseudo-gap in the conductance spectrum was observed in calculations with energy resolution of 35 meV, even upon large-angle asymmetric bending. Our calculations thus indicate that even moderate diameter armchair tubes essentially retain their metallic character even after large angle bending and can therefore be assigned to the (ii) class of behavior in Ref. [4].
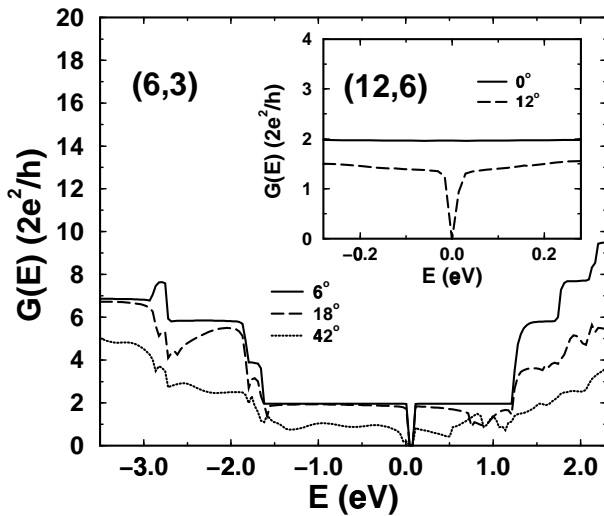

Figure 3: Conductance of a bent (6,3) chiral nanotube. Different curves correspond to different bending angles: 6°, 24°, and 42°, as shown in the legend. Inset: conductance of a bent (12,6) chiral nanotube for $\theta = 0°, 12°$. The Fermi energy is taken as reference.

In Fig. 3 we present the conductance of a bent (6,3) chiral nanotube, for $\theta = 6°, 18°$ and 42°. Because of the relatively small diameter ($d = 0.6$ nm), the curvature induced breaking of the degeneracy in the band structure opens a gap ($E_g \approx 0.1$ eV), clearly present in Fig. 3. For large deformations ($\theta = 42°$), this gap is widened ($E_g \approx 0.2$ eV), increasing the semiconducting character of the nanotube. One can then expect that bending in a large diameter, metallic chiral nanotube will drive it towards a semiconducting behavior. This behavior is actually computed for a (12,6) chiral tube ($d = 1.2$ nm), as shown in the inset of Fig. 3. A bending-induced gap of $\approx$ 60 meV is opened at a relatively small angle (12°), whereas the NT was perfectly conducting prior to bending. This result demonstrates that local barriers for electric transport in metallic chiral NT's can occur with no defect involved and just be due to a deformation in the tube wall. Given the relatively small values of the energy gaps, the conductance will be affected only at low temperatures, leading to the assignment of these tubes to the (iii) class of behavior in Ref. [4].

Although bending by itself can already cause a significant change in the electrical properties, defects are likely to form in a bent or a deformed nanotube, because of the strain occurring during the bending process [18]. It is now well established that a carbon nanotube under tension releases its strain via the formation of topological defects [1]. We have investigated how these defects affect the conductance of metallic armchair nanotubes of different diameters. Table I summarizes our results for (5,5) and (10,10) NT's under 5% strain, both

4

	pristine	(5–7–7–5)	(5–7)–(7–5)	(5–7–8–7–5)
(5,5)	2.00	1.70	1.11	1.26
(10,10)	2.00	1.85	1.33	1.72

Table I. Conductances of armchair nanotubes with point defects. (5-7-7-5) is the Stone-Wales defect; (5-7)-(7-5) corresponds to the onset of plastic behavior with the two (5-7) pairs separated by one row of hexagons; (5-7-8-7-5) corresponds to the onset of brittle behavior, with the opening of a higher order carbon ring, see text. In units of $2e^2/h$.

pristine and in the presence of different topological defects: (i) a (5-7-7-5) defect, obtained via the rotation of the C-C bond perpendicular to the axis of the tube; (ii) a (5-7) pair separated from a second (7-5) pair by a single hexagon row, as in the onset of the plastic deformation of the nanotube [1]; and (iii) a (5-7-8-7-5) defect, where another bond rotation is added to the original (5-7-7-5) defect, producing a higher order carbon ring (onset of the brittle fracture) [1]. While strain alone does not affect the electronic conduction in both tubes, the effect of defects on conductance is more evident in the small diameter (5,5) NT, while it is less pronounced in the larger (10,10) NT. Our results for the (10,10) tube with a single (5-7-7-5) defect compare very well with a recent *ab initio* calculation [12]. If more than one (5-7-7-5) defect is present on the circumference of the NT, the conductance at the Fermi level is lowered: for the (10,10) NT it decreases from 2 ($2e^2/h$) to 1.95, 1.70 and 1.46 ($2e^2/h$) for one, two or three defects, respectively.

The decrease in conductance is accompanied by a small increase in the DOS at the Fermi energy. This is due to the appearance of defect states associated with the pentagons and heptagons within the metallic plateau near the Fermi level. These localized states behave as point scatterers in the electronic transmission process and are responsible for the decrease in conductance [19]. This result confirms that in large diameter nanotubes the key quantity in determining the electrical response is the density of defects per unit length. This is also in agreement with recent measurements of Paulson *et al.* [5] of the electrical properties of carbon nanotubes under strain applied with an AFM probe. As the AFM tip pushes the tube, the strain increases without any change in the measured resistance until the onset of a structural transition is reached. This corresponds to the beginning of a plastic/brittle transformation that releases the tension in the NT [1] and coincides with a sharp yet finite increase in resistance. Since the onset of the plastic/brittle transformation that precedes the breakage is associated with the formation of a region of high defect density [1], the conductance at the Fermi energy is drastically reduced.

Optical spectroscopy of hydrogenated Si surfaces

The optical spectroscopy of surfaces, in particular reflectance anisotropy/difference spectroscopy (RAS/RDS), is an extremely versatile tool of surface analysis [20, 21]. However, the anisotropy spectra are difficult to interpret and provide only indirect information. Only a strong interaction between experimental and theoretical efforts allows for a full exploitation of the potential of RAS. The theoretical progress has been hampered, however, by the large numerical expense required for converged calculations of surface optical properties. Thanks to the development of both computational techniques and resources, we have recently suc-
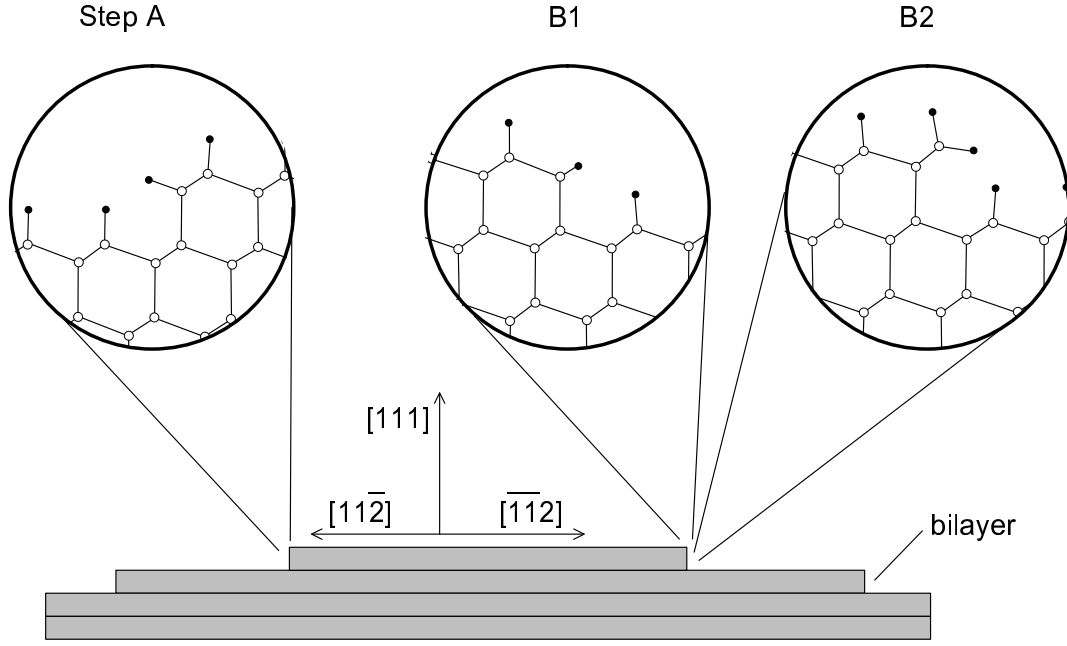
Figure 4: Side view of the relaxed step configurations studied in this work. Empty (filled) circles represent Si (H) atoms.

ceded in calculating anisotropy spectra from *first principles* in quantitative agreement with the measured data [22, 23]. Such calculations are very involved, however, and have up to now been restricted to ideal surfaces. Realistic surfaces, and growth structures in particular, however, are characterized by defects such as surface steps, which give rise to distinct optical anisotropies [24, 25, 26]. The theoretical description of these step-related optical anisotropies is thus important in the context of the correct interpretation of RAS spectra measured during growth. Therefore we extended our earlier studies on ideal surfaces [22, 23, 27, 28, 29] to defect structures and investigated, to our knowledge for the first time, the influence of surface steps on the optical anisotropy from *first principles*. As a first step in that direction we chose the stepped Si(111):H surface [30], whose geometry is well known from experiment and whose optical properties have been measured in detail [24]. For comparison we also performed calculations on Si(110):H.

As an example of step-induced optical anisotropies we study bilayer steps at the hydrogenated Si(111) surface. The two principal directions of miscut for this surface are $<11\bar{2}>$ and $<\bar{1}\bar{1}2>$. Assuming straight steps and barring any reconstruction, the first miscut (A in Fig. 4)

gives step atoms with one dangling bond each, and the second with two dangling bonds each. In the latter case two different atomic structures are possible: a dihydride structure forms that either lies in a plane parallel (B1 in Fig. 4) or perpendicular to the step edge (B2). All surface bonds are saturated by hydrogen. The Si atoms thus remain in bulk-like configurations and the relaxations are rather small and local. We find that the formation of a vertical dihydride structure in a plane perpendicular to the step edge (B2 in Fig. 4) is energetically preferred to the B1 configuration. This finding agrees with the results of

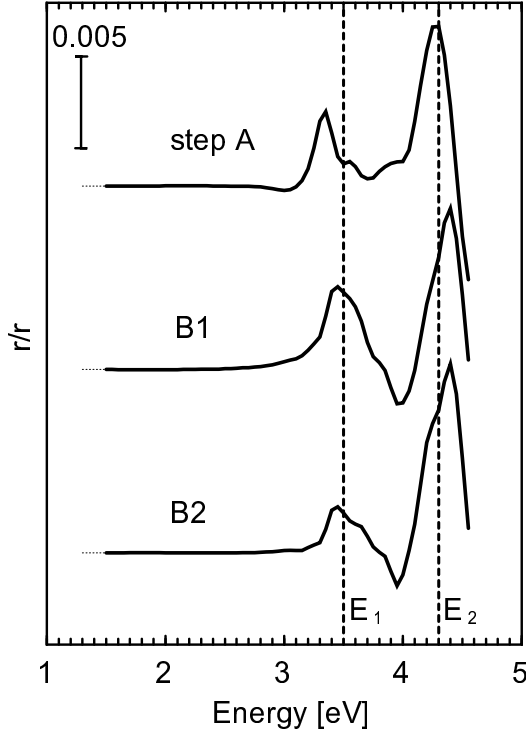6

infrared [31] and Raman spectroscopy [32].

Figure 5: Calculated RAS for Si step geometries shown in Fig. 4. Bulk CP energies are indicated.

The calculated RAS spectra for the three investigated step geometries are presented in Fig. 5. All steps give rise to strong anisotropy features close to the bulk critical point (CP) energies. The main differences between the spectrum calculated for $<11\bar{2}>$ and $<\bar{1}\bar{1}2>$ steps are a blueshift of about 0.1 eV and the occurrence of negative anisotropies at around 3 eV for the former and at around 4 eV for the latter two spectra. Based on the striking similarity of the measured step-induced RAS to that of Si(110):H, it was suggested in Ref. [24] that the optical response of $<11\bar{2}>$ steps arises from the (110)-like regions of the stepped surface.

Fig. 6 shows the calculated spectrum for the Si(110):H surface. It is indeed rather similar to the RAS induced by $<11\bar{2}>$ steps: Maxima appear at the CP energies and there is an additional shallow minimum around 3 eV. The line shape, however, in particular around the E_1 energy, is different from that calculated for the step configuration and the relative ratio of the anisotropies at the E_1 and E_2 CP energies is smaller. Furthermore, the overall similarity of the calculated RAS for all investigated step configurations suggests that one cannot explain the optical response of the $<11\bar{2}>$ stepped surface solely in terms of their (110)-like regions.
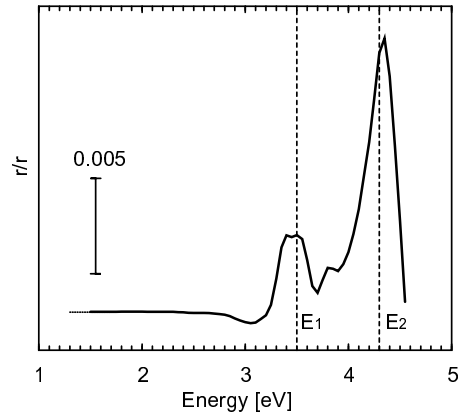
The overall similarity of all calculated step spectra indicates that the reflectance anisotropy originates from the perturbation of bulk wave functions by the formation of surface steps, rather than from electronic transitions between step-localized surface states. This picture is corroborated by our analysis separating spatially the contributions to the RAS (see Ref. [30]): Electronic transitions within the uppermost 8 Å of the surface only modify the spectra, whose main features arise from transitions in deeper layers.

The calculated spectrum for Si(110):H (Fig. 6) is interesting in its own right. It clearly resembles the imaginary part of the dielectric function of Si. It is at variance with the tight-binding results of

Figure 6: Calculated RAS for Si(110):H. Bulk CP energies are indicated.

Ref. [33], but agrees well with experiment [24]. In Ref. [33] it was concluded that the existence of Si and H vacancies at the Si(110):H surface is a necessary condition for calculating line shapes in rough agreement with experimental data. Furthermore, it was stated that the

7

surface local-field effect has to be included to obtain reasonable agreement with experiment. Our results, however, show that even an ideal Si(110):H surface gives rise to a dielectric function-like RAS spectrum. We do not find any indication for a particular importance of the surface local-field effect for that surface.

A direct comparison of the data calculated for stepped surfaces with experiment is not possible, as the existing measurements [24] were performed on surfaces with considerably smaller step densities. Unfortunately, the lateral periodicities needed to accommodate wider terraces are still out of reach for *ab initio* calculations of the optical response. In Ref. [24] it was noted, however, that the anisotropy signal for Si(111):H vicinally cut toward $[11\bar{2}]$ depends nearly linearly on the step density. A similar dependence was recently obtained for Si(001) [26]. Furthermore, our results, as well as earlier work [34], show that the atomic relaxations of the step edges are rather small and local. Therefore, it is expected that our calculations can be extrapolated to allow for a meaningful comparison with the measured data.
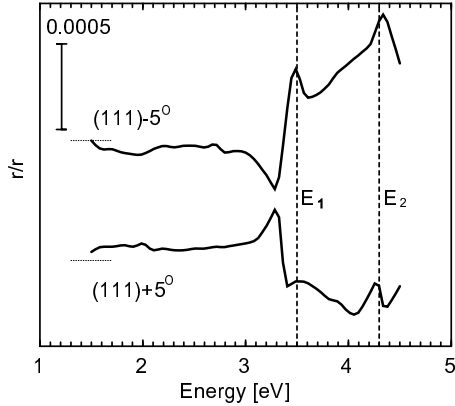

Figure 7: Measured RAS [24] for vicinally cut Si(111):H surfaces.

In Fig. 7 we show the experimental data [24] for surfaces vicinally cut $\pm5°$. The upper curve in Fig. 7 shows the RAS of the surface cut toward $[11\bar{2}]$. The main characteristics of the spectrum are the pronounced anisotropy maxima near the E_1 and E_2 CPs of the bulk band structure. This is in qualitative agreement with the corresponding calculated spectrum for $<11\bar{2}>$ steps (A in Fig. 4). The measured anisotropies are about one order of magnitude smaller than the calculated values. This can be explained partially by the lower step density. Temperature effects and sample imperfections neglected in our calculation also reduce the measured anisotropy signal. The neglect of excitonic effects in the calculations leads to differences in the line shape between the measured and calculated RAS spectra, in particular around the E_1 energy. If these limitations are borne in mind, however, the agreement between experiment and theory for the $<11\bar{2}>$ step-induced optical anisotropy is satisfactory.

This is seemingly not the case for $<\bar{1}\bar{1}2>$ steps. The lower curve in Fig. 7 shows data measured for the Si(111):H surface miscut 5° toward $[\bar{1}\bar{1}2]$. Yasuda *et al.* [24] assumed that the measured anisotropy is induced by bilayer $<\bar{1}\bar{1}2>$ steps. This interpretation does not agree with the calculations. Theory predicts positive anisotropy features at the E_1 and E_2 energies, while the measured anisotropies are negative. It is implausible that the calculations should yield a qualitatively wrong result. From Fig. 7 it seems as if the (111)+5° spectrum were an inverted and somewhat reduced version of the (111)-5° spectrum. By means of infrared [31, 35] and Raman spectroscopy [32], as well as STM measurements [36, 37], it has been demonstrated that the atomic structures of Si(111):H surfaces miscut toward $[\bar{1}\bar{1}2]$ depend strongly on the preparation conditions. In particular, a transformation of straight dihydride-terminated $<\bar{1}\bar{1}2>$ steps into a staircase-like arrangement of monohydride terminated $<11\bar{2}>$ steps was observed. These newly formed steps form angles of 60/120° with the original step edges. Assuming a complete transformation of straight $<\bar{1}\bar{1}2>$ steps into

8

zig-zag chains of ideal $<11\bar{2}>$ steps, the optical anisotropy of the surface should from pure geometrical considerations correspond to the anisotropy measured for straight $<11\bar{2}>$ steps, but multiplied by $-\sqrt{3}$. In reality, the optical anisotropy of remaining, not-transformed parts of $<\bar{1}\bar{1}2>$ steps will partially cancel the signal from the zig-zag chains. A further disturbance of the "ideal" RAS spectrum can be expected from contributions due to the edges of the staircase structures. Thus, it seems likely that the optical spectrum of a Si(111):H surface miscut toward $[\bar{1}\bar{1}2]$ is an inverted, reduced and somewhat disturbed version of the spectrum measured for a surface miscut toward $[11\bar{2}]$. Obviously, the actual spectrum will depend on the preparation conditions. This hypothesis, if correct, gives a natural explanation of the experimental findings of Ref. [24], which are seemingly at odds with our calculations. However, further experiments are needed to verify the suggested interpretation.

References

[1] M. Buongiorno Nardelli, B.I. Yakobson and J. Bernholc, Phys. Rev. B **57**, R4277 (1998); Phys. Rev. Lett. **81**, 4656 (1998).

[2] See, for instance, M.R. Falvo, G.J. Clary, R.M. Taylor II, V. Chi, F.P. Brooks Jr., S. Washburn and R. Superfine, Nature **389**, 582 (1997).

[3] P.G. Collins, A. Zettl, H. Bando, A. Thess and R. Smalley, Science **278**, 100 (1996); S.N. Song, X.K. Wang, R.P.H. Chang and J.B. Ketterson, Phys. Rev. Lett. **72**, 697 (1994); L.Langer, L. Stockman, J.P. Heremans, V. Bayot, C.H. Olk, C. Van Haesendonck, Y. Bruynseraede and J.-P. Issi, J. Mater. Res. **9**, 927 (1994); L.Langer, V. Bayot, E. Grivei, J.-P. Issi, J.P. Heremans, C.H. Olk, L. Stockman, C. Van Haesendonck and Y. Bruynseraede, Phys. Rev. Lett. **76**, 479 (1996); S.J. Tans, M.H. Devoret, H. Dai, A. Thess, R.E. Smalley, L.J. Georliga and C. Dekker, Nature **386**, 474 (1997); A. Bachtold, C. Strunk, J.-P. Salvetat, J.-M. Bonnard, L. Forró, T. Nussbaumer and C. Schönenberger, Nature **397**, 673 (1999).

[4] A. Bezryadin, A.R.M. Verschueren, S.J. Tans and C. Dekker, Phys. Rev. Lett. **80**, 4036 (1998).

[5] S. Paulson, M.R. Falvo, N. Snider, A. Helser, T. Hudson, A. Seeger, R.M. Taylor II, R. Superfine and S. Washburn, http://xxx.lanl.gov/abs/cond-mat/9905304, preprint (1999).

[6] W. Tian and S. Datta, Phys. Rev. B **49**, 5097 (1994).

[7] R. Saito, G. Dresselhaus, M.S. Dresselhaus, Phys. Rev. B **53**, 2044 (1996).

[8] L. Chico, L.X. Benedict, S.G. Louie and M.L. Cohen, Phys. Rev. B **54**, 2600 (1996).

[9] R. Tamura and M. Tsukada, Phys. Rev. B **55**, 4991 (1997); *ibid*, **58**, 8120 (1998).

[10] M.P. Anantran and T.R. Govindan, Phys. Rev. B **58**, 4882 (1998).

[11] A.A. Farajian, K. Esfarjani and Y. Kawazoe, Phys. Rev. Lett. **82**, 5084 (1999).

[12] H.J. Choi and J. Ihm, Phys. Rev. B **59**, 2267 (1999).

[13] A. Rochefort, F. Lesage, D.R. Salahub and P. Avouris, http://xxx.lanl.gov/abs/cond-mat/9904083, preprint (1999).

[14] M. Buongiorno Nardelli, Phys. Rev. B, **60**, 7828 (1999).

[15] See, for instance, M.S. Dresselhaus, G. Dresselhaus and P.C. Eklund, *Science of fullerenes and carbon nanotubes* (Academic Press, San Diego, 1996). We do not discuss the many-body effects that may lead to insulating behavior at temperatures near 0 K.

[16] X. Blase, L.X. Benedict, E.L. Shirley and S.G. Louie, Phys. Rev. Lett. **72**, 1878 (1994).

[17] J. Ihm and S.G. Louie, private communication (1999).

[18] M. Buongiorno Nardelli and J. Bernholc, unpublished (1999).

[19] V.H. Crespi, M.L. Cohen and A. Rubio, Phys. Rev. Lett. **79**, 2093 (1997).

[20] D. E. Aspnes, Surf. Sci. **309**, 1017 (1994).

[21] W. Richter and J. T. Zettler, Appl. Surf. Sci. **101**, 465 (1996).

[22] W. G. Schmidt, N. Esser, A. M. Frisch, P. Vogt, J. Bernholc, F. Bechstedt, M. Zorn, T. Hannappel, S. Visbeck, F. Willig, and W. Richter, Phys. Rev. B. (accepted).

[23] W. G. Schmidt, J. L. Fattebert, J. Bernholc, and F. Bechstedt, Surf. Rev. Lett. **6**, 1159 (1999).

[24] T. Yasuda, D. E. Aspnes, D. R. Lee, C. H. Bjorkman, and G. Lucovsky, J. Vac. Sci. Technol. A **12**, 1152 (1994).

[25] L. Mantese, U. Rossow, and D. E. Aspnes, Appl. Surf. Sci. **107**, 35 (1996).

[26] S. G. Jaloviar, J.-L. Lin, F. Liu, V. Zielasek, L. McCaughan, and M. G. Lagally, Phys. Rev. Lett. **82**, 791 (1999).

[27] N. Esser, W. G. Schmidt, J. Bernholc, A. M. Frisch, P. Vogt, M. Zorn, M. Pristovsek, W. Richter, F. Bechstedt, T. Hanappel, and S. Visbeck, J. Vac. Sci. Technol. B **17**, 1691 (1999).

[28] A. M. Frisch, W. G. Schmidt, J. Bernholc, M. Pristovsek, N. Esser, and W. Richter, Phys. Rev. B **60**, 2488 (1999).

[29] W. G. Schmidt, E. L. Briggs, J. Bernholc, and F. Bechstedt, Phys. Rev. B **59**, 2234 (1999).

[30] W. G. Schmidt and J. Bernholc, Phys. Rev. B **61**, 7604 (2000).

[31] P. Jakob, Y. J. Chabal, K. Raghavachari, R. S. Becker, and A. J. Becker, Surf. Sci. **275**, 407 (1992).

[32] M. A. Hines, Y. J. Chabal, T. D. Harris, and A. L. Harris, J. Chem. Phys. **101**, 8055 (1994).

[33] B. S. Mendoza, R. Del Sole, and A. I. Shkrebtii, Phys. Rev. B **57**, R12709 (1998).

[34] X.-P. Li, D. Vanderbilt, and R. D. King-Smith, Phys. Rev. B **50**, 4637 (1994).

[35] P. Jakob and Y. J. Chabal, J. Chem. Phys. **95**, 2897 (1991).

[36] G. J. Pietsch, U. Köhler, and M. Henzler, J. Appl. Phys. **73**, 4797 (1993).

[37] J. Flidr, Y.-C. Huang, T. A. Newton, and M. A. Hines, Chem. Phys. Lett. **302**, 85 (1999).